Compression of the MoM Matrix Using Macrobasis Functions with a Full-Controlable Accuracy

J.M. Tamayo [#1], A. Heldring [#2], J.M. Rius [#3]

[#] *Dept. of Signal Theory & Comm, Polythecnic University of Catalonia, c/ J. Girona 1, 08034, Barcelona, Spain*

[1] jose.maria.tamayo@tsc.upc.edu

[2] heldring@tsc.upc.edu

[3] rius@tsc.upc.edu

***Abstract*— A new accuracy-controlable method for compressing the MoM impedance matrix of an electromagnetic problem based on a basis change plus a truncation with a threshold is presented here. The idea is to switch to singular basis functions, which are defined on relatively large subdomains of the object, representing perfectly the far field of the subdomain and yielding compression for well-separated blocks. Although the construction of the matrix is not computationally efficient compared with other matrix compression methods, it is still quite interesting from a theoretical point of view. Furthermore, it clearly explains certain characteristics of some of those methods, particularly the errors in the solution of those based in pseudoglobal functions.**

I. Introduction

In recent years, several methods have been proposed to accelerate the solution of electromagnetic scattering and radiation problems using the Method of Moments (MoM). These methods are based on approximating the interactions between two sets of separated basis functions. In this paper we introduce two new techniques using an idea from [1] to recompress the matrix obtained from these methods and therefore accelerating the matrix-vector product. The first technique (Sec. II-A) will introduce moderate errors acceptable for a whole range of applications. However, for a more accurate results it will be generalized in section II-B. The second method is, however, more time consuming.

When the object is split in different subdomains, many of the existing methods (ACA [2], MDA-SVD [3], ...) try to compress the matrix corresponding to the interaction between each pair of boxes separatedly. However, in this case for each box we try to find a common pattern with all the other boxes of the space. This common part will be related with the far field produced by the isolated box. Firstly, it seems to lead to a very effective way of proceeding, although finally it will not be like this because we need to do too many matrix-matrix products.

II. Theory

For the sake of simplicity let us start with the description of the technique for a single scale iterative algorithm although it will be immediately generalized to the multiscale one. Imagine we have subdivided the MoM matrix Z in blocks corresponding to different subdomains of the object under study as follows (single scale, see Fig. 1):

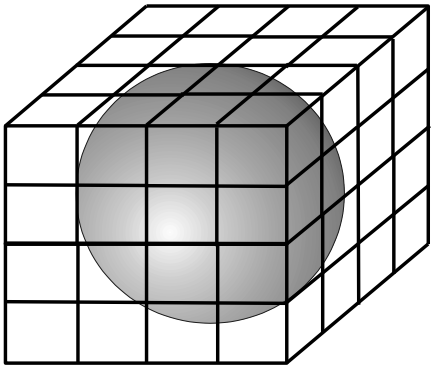

Fig. 1. Representation of a single level subdomain decomposition.

$$\begin{bmatrix} E_1 \\ E_2 \\ \vdots \\ E_M \end{bmatrix} = \begin{bmatrix} Z_{11} & Z_{12} & \cdots & Z_{1M} \\ Z_{21} & Z_{22} & \cdots & Z_{2M} \\ \vdots & \vdots & \ddots & \vdots \\ Z_{M1} & Z_{M2} & \cdots & Z_{MM} \end{bmatrix} \begin{bmatrix} J_1 \\ J_2 \\ \vdots \\ J_M \end{bmatrix} \tag{1}$$

or $E = ZJ$, where E is the excitation vector, while J is the current vector or the unknowns. The blocks Z_{ij} should be considered not as a matrix but as a product of different matrices in a compressed form, for instance using ACA [2] or MDA-SVD [3] techniques. We introduce now a set of orthogonal matrices V_i, one per block with $i = 1, \ldots, M$, which will transform the MoM matrix into $Z'_{ij} = V_i^H Z_{ij} V_j$. In a matrix form, it can be expressed with the introduction of a block-diagonal orthogonal matrix V

$$V = \begin{bmatrix} V_1 & & & \\ & V_2 & & \\ & & \ddots & \\ & & & V_M \end{bmatrix} \tag{2}$$

as a new linear system $E' = Z'J'$, from now on called the transformed system, where:

$$\begin{aligned} E' &= V^H E \\ Z' &= V^H Z V \\ J' &= V^H J \end{aligned} \tag{3}$$

This is the system we want to compress and for doing so, two techniques will be described, but before seing them let us introduce which are those matrices V_i. Observe that they can be seen as a basis change between the RWG basis functions and some subdomain basis functions which are defined in the whole block under study. They should sort by importance the contribution to the matrix. As they need to be common for the interaction with the rest of the blocks, they must be related with the far field produced by the block isolated. A first option, and the one is used in [1] for the FMM, is to consider the aggregation matrix F_n of the FMM representing the radiation pattern on the Ewald sphere due to each basis function within a group, and apply a singular value decomposition (SVD). Then we define V_i as the orthogonal right outer matrix obtained from that decomposition. It means we are switching to a set of singular basis functions. Another way to proceed, which lead us to the same results, is to take the interaction matrix between the samples in the block and some equivalent functions covering the far field of that block, for instance distributed on a sphere with a sufficiently large radius. Then we apply the same procedure as above with the matrix F_n obtaining a new set of singular basis functions. The reason they bring us to the same results is that both cases represent the far field.

A. First Approach: PseudoGlobal Basis Elimination

Let us see a first way to obtain a further compressed version of the new system matrix Z'. For each block Z_{ij} with $i \neq j$, i.e. each non-self-interaction submatrix, $Z'_{ij} = V_i^H Z_{ij} V_j$. Assume that we can subdivide V_i and V_j into significant (superscript 1) and non-significant (superscript 2) sets of columns, assigning more significance to the ones whose singular values in the decomposition of the previous section are above a certain threshold:

$$\begin{aligned} V_i &= \begin{bmatrix} V_i^{(1)} & V_i^{(2)} \end{bmatrix} \\ V_j &= \begin{bmatrix} V_j^{(1)} & V_j^{(2)} \end{bmatrix} \end{aligned} \tag{4}$$

and substituting in the last equation we obtain:

$$\begin{aligned} Z'_{ij} &= \begin{bmatrix} V_i^{(1)H} Z_{ij} V_j^{(1)} & V_i^{(1)H} Z_{ij} V_j^{(2)} \\ V_i^{(2)H} Z_{ij} V_j^{(1)} & V_i^{(2)H} Z_{ij} V_j^{(2)} \end{bmatrix} \\ &\approx \begin{bmatrix} V_i^{(1)H} Z_{ij} V_j^{(1)} & 0 \\ 0 & 0 \end{bmatrix} \end{aligned} \tag{5}$$

where if the last approximation is valid (done in [1]), we have a compressed version of Z'_{ij}, as we only need to store the submatrix $V_i^{(1)H} Z_{ij} V_j^{(1)}$. We have eliminated the least important macrobasis functions for this set of interactions. If the two matrices V_i and V_j corresponded to the two orthogonal matrices in the SVD of Z_{ij} then Z'_{ij} would be exactly a diagonal matrix with the ordered singular values in the diagonal and the approximation would be optimum in terms of mean squares. But the fact is that V_i are and must be the same for all the matrices Z_{ij} and it will obviously introduce a new error to our algorithm.

To generalize the procedure to a multiscale algorithm we can compute the V_i corresponding to the finest level. For coarser levels we combine the V_i of the 'child' boxes at the finest level.

Unfortunately, the method outlined above introduces several problems: first of all, the compression should be very high for the method to be useful because besides the original matrix we also need to store the new matrix V and, if the original matrix was symmetric, the new matrix Z' is not symmetric anymore which multiplies the computational cost by two. Furthermore, the error introduced by this approximation is acceptable for far-field computations but not for parameters that depend directly on the surface current. The last problem, and probably the easiest to solve is that the preconditioner needs to be redefined so that it is adapted to the new system.

To overcome the problem with the error we introduce a second approach in the next section.

B. Second Approach: Threshold Truncation

The fact is that the macrobasis functions defined above in V have the necessary information to represent the far field sorted by importance. Therefore, to represent the field in another box the contribution of the first few singular functions or first columns of V is sufficient. Reciprocally, to well define the currents in the source box it is enough to know the field in the observation box due to the first few singular functions or columns of V^H. Thus the important information in the transformed matrix Z'_{ij} (considering the whole matrix V and not a truncated version of it) is distributed in the first columns and in the first rows and not only in the first quadrant of the matrix. This can be observed in Fig. 2 where if the required relative error is not very high, then it is possible to operate as in the first approach. However, if a more accurate result is necessary then we need to include a sparse version of the submatrix with the shape of an upside-down "L"(see Fig. 2 down right). This means that doing the whole transformation (3) with the same matrix V as in the previous section and removing all the elements which are below a certain threshold a good result with an unbounded accuracy is obtained. This will be illustrated with some numerical examples in section III.

In conclusion, if the matrix is truncated removing the least important macrobasis functions as in the first approach and as in many existing algorithms, there is a certain error which cannot be reduced unless the whole set of basis functions is used. These algorithms have a relatively good RCS behaviour but they do not fit exactly because the errors in J can be

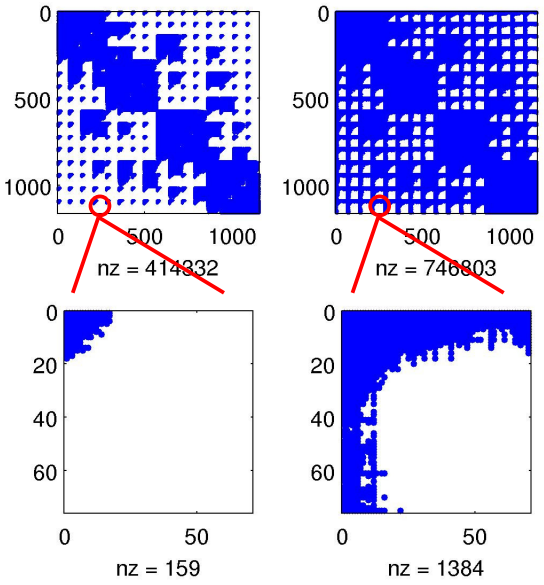

Fig. 2. Sparsity pattern of the transformed MoM matrix $Z' = V^H Z V$ for a square plate $2\lambda \times 2\lambda$ with $N = 1160$ unknowns and divided into $M = 16$ blocks. Truncation thresholds $\tau = 10^{-3}$ on the left and $\tau = 10^{-4}$ on the right. Below, one of the subblocks zoomed. The discretization sizes of the RWG elements are between $\lambda/10$ and $\lambda/7$.

too big. They only work well for far field parameters. If, on the other hand, we proceed as outlined in this section, this limitation is removed and the error in J can be made arbitrarily small, as will be seen in the following section.

III. Numerical Results

Several simulations have been performed to corroborate the theoretical error reduction with the threshold τ and how it behaves with the obtained compression factor of the matrix for each case. The compression factor shown here is computed with the following expression:

$$\text{Comp. Fact.} = \frac{N^2}{\text{Number of nonzero elements of } Z'} \tag{6}$$

The relative errors in the induced currents solution is computed as follows:

$$\epsilon = \frac{J_{ex} - J_{method}}{J_{ex}} \tag{7}$$

where J_{ex} is the exact or a very accurate solution of the MoM system and J_{method} are the currents obtained with the methods explained above. Observe that the errors are computed from the solution in the RWG basis functions and not in the transformed ones. Note also that although some results could have been compared to measured or theoretical results, they are not shown here. The reason is that the most important thing is the error introduced by the compression algorithm under study and not the error due to the discretization of the problem, which is very well-known by now.

The range of simulations comprises two canonical problems, a sphere and a square plate, and a more practical one, an X-band Horn.

Without having tried to optimize this parameter, in all the examples below a box radius of 0.5λ has been chosen. Remember that only the single-scale algorithm is implemented, and that is what the results correspond to.

A. Sphere

Four different spheres have been simulated with radius $R = 0.47\lambda$, $R = 0.93\lambda$, $R = 1.85\lambda$ and $R = 3.7\lambda$. The number of unknowns or of RWG basis functions is $N = 768$, $N = 3072$, $N = 12288$ and $N = 49152$ respectively. For each sphere different truncation thresholds τ have been tested, in order to observe the evolution of the two most important parameters, the relative error in J and the compression factor of the MoM matrix. Fig. 3 and Fig. 4 show the results.

To have a good comparison of the results, all the spheres studied here have been discretized with the same electric sizes, in particular the RWG edges are of about $\lambda/8$ of length.

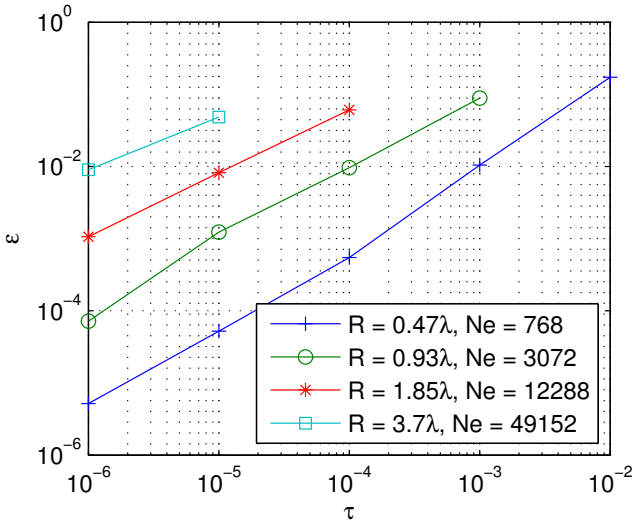

Fig. 3. Relative error in the currents solution vector J as a function of the truncation threshold τ for spheres of different electrical sizes using the truncation method. Discretization sizes of the RWG elements always around $\lambda/8$.

Fig. 3 contains a logarithmic plot which proves for every case that the relative error ϵ decreases regularly with the reduction of the threshold τ. This error reduction leads to a less compressed matrix and this is what is analyzed in Fig. 4. It is also clear that fixing a relative error ϵ, a better compression factor can be accomplished if the sphere or the object is electrically larger. This is logical as when the object is greater there are more and more distant blocks and many of them are much further from each other than in smaller cases.

To end with the spheres analysis, Fig. 5 and Fig. 6 display the bistatic RCS, plane E and plane H respectively, of the largest sphere with radius $R = 3.7\lambda$ and $N = 49152$. The results with and without compression completely overlap eachother in the figure..

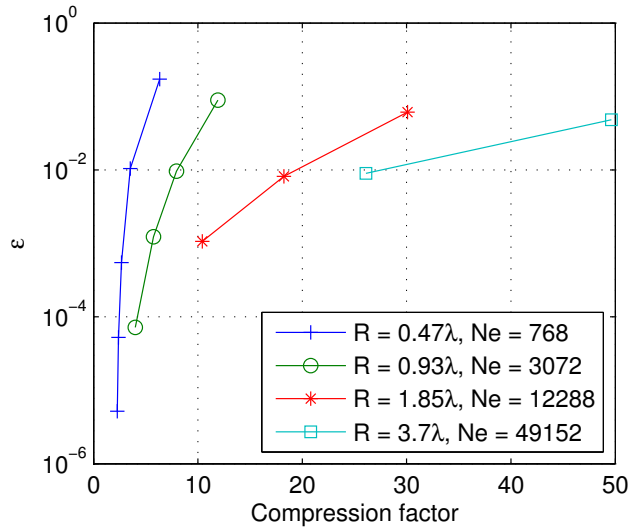

Fig. 4. Relative error in the currents solution vector J as a function of the compression factor defined in (6) for spheres of different electrical sizes using the truncation method. Discretization sizes of the RWG elements always around $\lambda/8$.

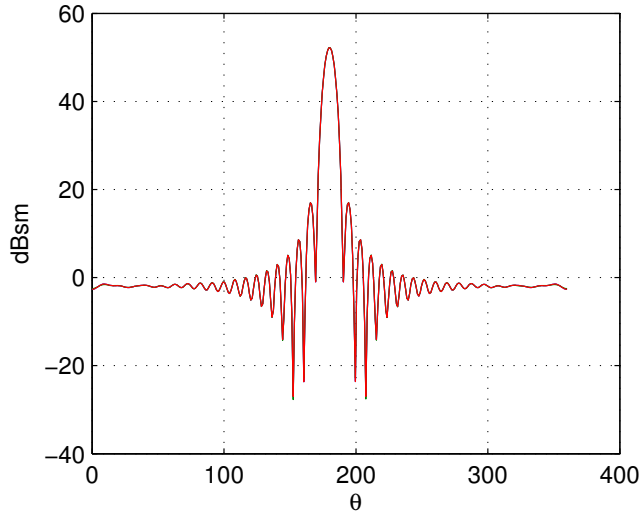

Fig. 5. Bistatic RCS in the E-Plane for a sphere with a radius $R = 3.7\lambda$ and $N = 49152$ unknowns. There are the plots for the exact solution and for the solution with the truncation method with two different thresholds $\tau = 10^{-5}$ and $\tau = 10^{-6}$. The three plots overlap entirely. Discretization sizes of the RWG elements always around $\lambda/8$.

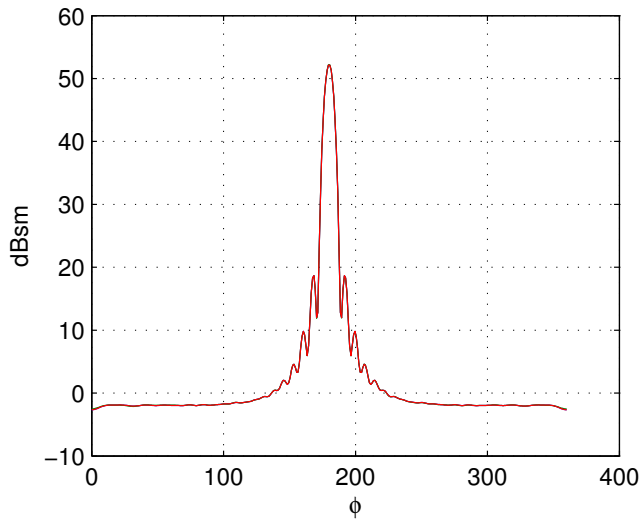

Fig. 6. Bistatic RCS in the H-Plane for a sphere with a radius $R = 3.7\lambda$ and $N = 49152$ unknowns. There are the plots for the exact solution and for the solution with the truncation method with two different thresholds $\tau = 10^{-5}$ and $\tau = 10^{-6}$. The three plots overlap entirely. Discretization sizes of the RWG elements always around $\lambda/8$.

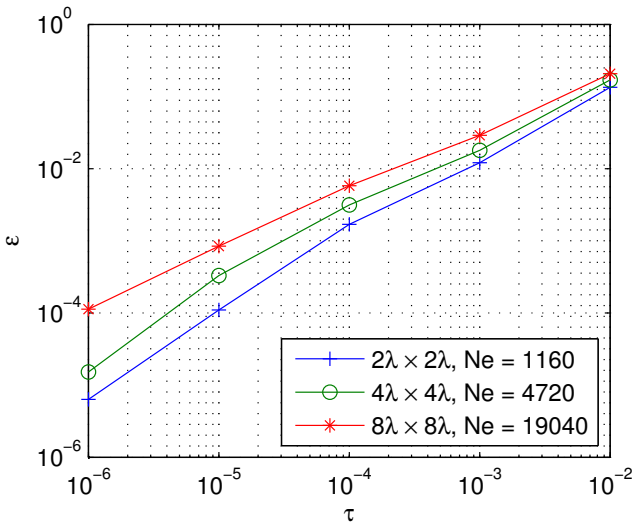

Fig. 7. Relative error in the currents solution vector J as a function of the truncation threshold τ for square plates of different electrical sizes using the truncation method. The excitation was a planewave from the broadside direction. Discretization sizes of the RWG elements always around $\lambda/8$.

B. Square Plate

Three square plates have been simulated of sizes $2\lambda \times 2\lambda$, $4\lambda \times 4\lambda$ and $8\lambda \times 8\lambda$ with $N = 1160$, $N = 4720$ and $N = 19040$ unknowns respectively. Following the same procedure as with the sphere, exactly the same conclusions can be extracted as is shown in Fig. 7 and Fig. 8.

C. X-Band Horn

An X-band pyramidal horn has been discretized into $N = 69228$ RWG basis functions with an average edge size of 0.18λ. The horn is fed by a rectangular monomode waveguide of length 2λ with an elementary dipole excitation at the center. The pyramidal section has a length of 8λ and the aperture size is $3\lambda \times 4\lambda$. The shape and induced current solution can be found in Fig. 9.

TABLE I
X-BAND HORN ERROR AND COMPRESSION

Threshold τ	10^{-3}	10^{-4}	10^{-5}
Relative Error ϵ **(%)**	4.5	1.3	0.6
Compression factor	24.4	17.2	8.3

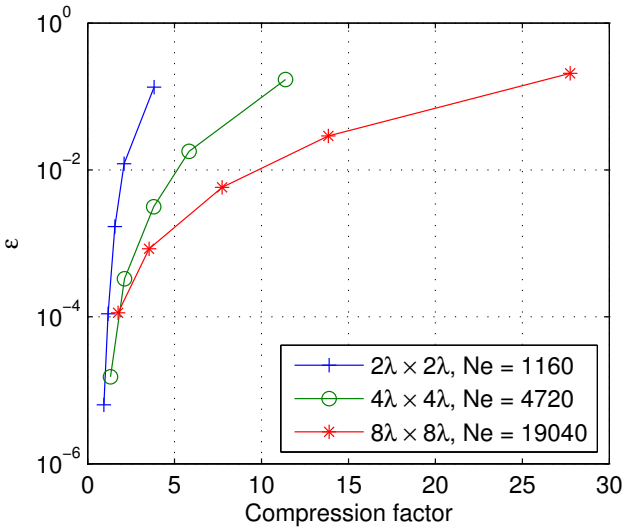

Fig. 8. Relative error in the currents solution vector J as a function of the compression factor defined in (6) for square plates of different electrical sizes using the truncation method. The excitation was a planewave from the broadside direction. Discretization sizes of the RWG elements always around $\lambda/8$.

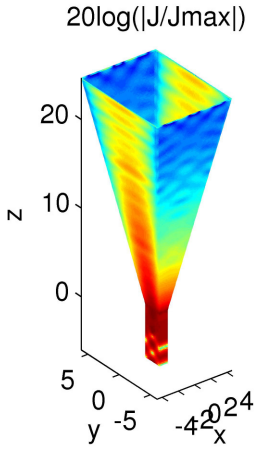

Fig. 9. Induced current in the surface of the X-band horn.

Table I shows the relative error in J and the compression factor of the matrix for different truncation thresholds τ (10^{-3}, 10^{-4} and 10^{-5}). Again it is clear that one can reduce the relative error in J by just decreasing the threshold τ, with the obvious negative effect of compressing less. Anyway, a good accuracy of about 1% can be achieved with a reasonable compression factor taking into account that the algorithm under study is a single-scale one.

IV. Conclusions

Two techniques and several results in the matter of compressing the MoM impedance matrix have been presented. Highly accurate results are possible if necessary just changing the threshold parameter τ used in the sparsification of the matrix. Some explanation of the poor accuracy in some existing methods has been done.

Acknowledgment

This work was supported in part by the Spanish Interministerial Commission on Science and Technology (CICYT) under projects TEC2006-13248-C04-02/TCM and TEC2007-66698-C04-01/TCM and CONSOLIDER CSD2008-00068 and by the "Ministerio de Educación y Ciencia" through the FPU fellowship program.

References

[1] J. L. Rodriguez, J. M. Taboada, M. G. Araújo, F. Obelleiro, L. Landesa, and I. García-Tunón, "On the use of the singular value decomposition in the fast multipole method," *IEEE Trans. Antennas Propagat, special issue on Large and Multiscale Computational Electromagnetics*, vol. 56, no. 8, pp. 2325–2334, Aug. 1998.

[2] M. Bebendorf, "Approximation of boundary element matrices," *Numer. Math.*, vol. 86, no. 4, pp. 565–589, 2000.

[3] J. M. Rius, J. Parrón, A. Heldring, J. M. Tamayo, and E. Úbeda, "Fast iterative solution of integral equations with method of moments and matrix decomposition algorithm singular value decomposition," *IEEE Trans. Antennas Propagat, special issue on Large and Multiscale Computational Electromagnetics*, vol. 56, no. 8, pp. 2314–2324, Aug. 1998.